SPE-201538-MS

Evaluating Perforation Erosion and its Effect on Limited Entry by Distributed Acoustic Sensor DAS Monitoring

Julia Pakhotina, Ding Zhu, and A. Daniel Hill, Texas A&M University

This paper was prepared for presentation at the SPE Annual Technical Conference & Exhibition originally scheduled to be held in Denver, Colorado, USA, 5 – 7 October 2020. Due to COVID-19 the physical event was postponed until 26 – 29 October 2020 and was changed to a virtual event. The official proceedings were published online on 21 October 2020.

Abstract

Limited entry is used in multistage fracturing to attempt to distribute fracture fluid among multiple perforation clusters evenly. As the slurry is pumped through perforations, the perforation holes can be eroded because of abrasion by the proppant, and therefore become enlarged, resulting in less effective limited entry and lower efficiency of the fracture treatment. Distributed Acoustic Sensing (DAS) is a method used for monitoring of fluid flow during hydraulic fracturing. By evaluating the changing DAS responses at perforation cluster locations during fracture pumping, DAS can be used to evaluate perforation erosion. DAS is a measurement of acoustic energy induced by fluid movement with fiber optic sensing cables. A raw acoustic signal recorded by the interrogator is transformed into an energy response (Frequency Band Energy), which is used for further interpretation of fluid volume distribution among perforated clusters on each stage of the fracturing treatment.

Based on previous laboratory experiments and computational simulations, there is a correlation between the Frequency Band Energy and fluid flow rate. As the flow rate is a function of fluid velocity and perforation area (diameter of perforation), the same flow rate could be attained with a combination of different velocities and areas, leading to a non-unique solution when interpreting DAS measurements. We transferred the correlation into the relationship between velocity and Frequency Band Energy, using the perforation area as an additional parameter. It enforces avoiding non-unique solutions in the interpretation process.

Perforation diameter is a function of erosion rate, which depends on the proppant concentration and velocity of fluid passing through the perforation. In order to connect correlation parameters with the diameter of perforations, computational simulations of fluid injection were conducted with different perforations geometries. Based on these simulations, a function that connects the area of perforation with a correlation parameter was obtained. It allows us to include the diameter of perforation in the analytical equation explicitly.

The application of the enhanced correlation in the interpretation process leads to increased accuracy of the fluid distribution calculation. For each time step, the velocity of the fluid, the mass of proppant, and the diameter of the perforations are computed, allowing the calculation of the flow rate in each perforation cluster. Perforation erosion is included in the model. Examples using field data are presented in the paper.

Introduction

The DAS based interpretation method for multistage hydraulic fracturing diagnosis, presented by Pakhotina et al. (2020), was constructed on the basis of the correlation (Chen et al., 2015; Pakhotina et al., 2017) between the sound pressure level of the flow-induced acoustic signal, L_{SP}, and flow rate, q, with parameters of correlation A and B:

$$\log(q^3) = A \times L_{SP} + B \tag{1}$$

The interpretation method is described by the system of Equations (2):

$$\begin{cases} N_1 q_1(t) = & N_1 10^{\frac{A_1}{3}E_1(t)} * \dfrac{q_T(t)}{\left(N_1 10^{\frac{A_1}{3}E_1(t)} + \cdots + N_n 10^{\frac{A_n}{3}E_n(t)}\right)} \\ N_n q_n(t) & = N_n 10^{\frac{A_n}{3}E_n(t)} * \dfrac{q_T(t)}{\left(N_1 10^{\frac{A_1}{3}E_1(t)} + \cdots + N_n 10^{\frac{A_n}{3}E_n(t)}\right)} \end{cases} \tag{2}$$

where N_i – number of perforations per cluster, q_i – the flow rate in one perforation in cluster i, E_i – frequency band energy in cluster i, q_T – the total flow rate during the injection procedure, A_i – parameters of correlation. This system of equations allows calculating flow rate in each perforation cluster at each time step and further cumulative volume of fluid distribution for each fractured stage. In this method, an assumption was made that the diameter of perforations in fractured clusters are equal before and during all period of injection. However, it does not correspond to the real situation as the initial diameter could vary from perf to perf before starting the hydraulic fracturing process. Also, the proppant movement through perforation holes provokes perforation erosion and subsequent a growth of perforation diameters.

In real field hydraulic fracturing treatments, the diameter of perforations is not equal for different perforation clusters because of variation in the initial perforating procedure (mainly caused by the uniformity of charges, the distance between perforating gun and the casing wall), and because pumping of proppant causes enlargement of perforation diameter due to erosion effect. Thus, the first question to answer in this study is if the linear relationship presented in equations 1 and 3 is still valid when perforation diameter becomes a variable. An initial numerical investigation was conducted using the computational fluid dynamics (CFD) approach for different perforation diameters. The relationships of $log(q^3)$ and L_{SP} by the numerical experiments for different perforation diameters are shown in Figure 1.

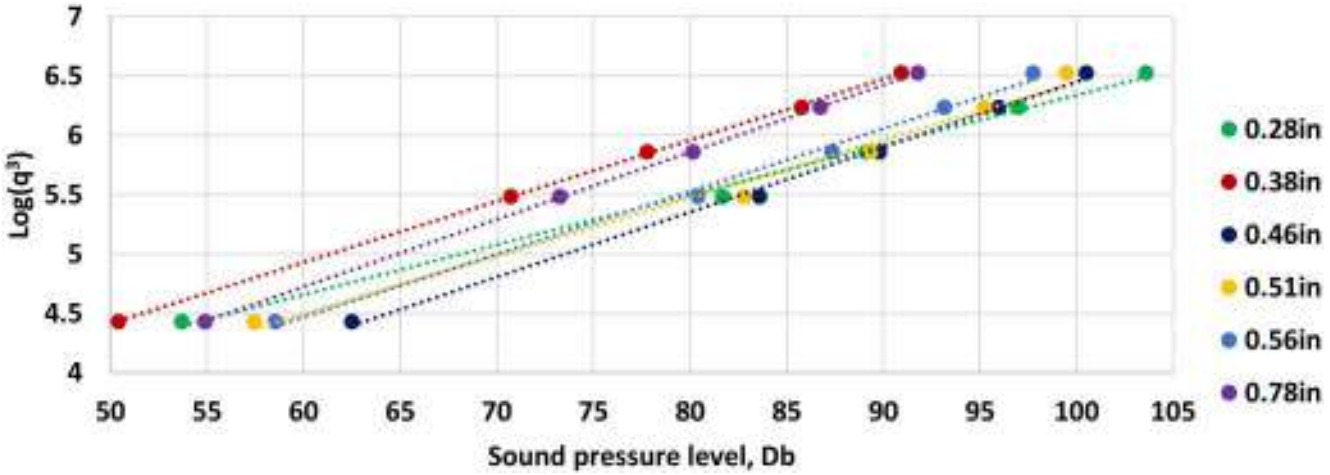

Figure 1—Effect of perforation diameter on the correlation between the acoustic signal and flow rate for water injection

From all these lines, it is concluded that all perforation sizes provide linear correlation, but correlation coefficients, slope A and intercept B, showed in Table 1, do not have a consistent dependency on the diameter as some of these lines cross each other.

Table 1—Parameters of correlation for water injection

Perforation diameter, in	A	B
0.28	0.042	2.1366
0.38	0.0515	1.8379
0.46	0.0548	0.9711
0.51	0.0489	1.5624
0.56	0.0529	1.2947
0.78	0.0567	1.3203

Assuming that parameter A depends on the diameter of the perforation tunnel, and based on the variation of the diameter, the correlation between A and logarithm of the cross-section area of perforation A_p is obtained, as shown in Figure 2.

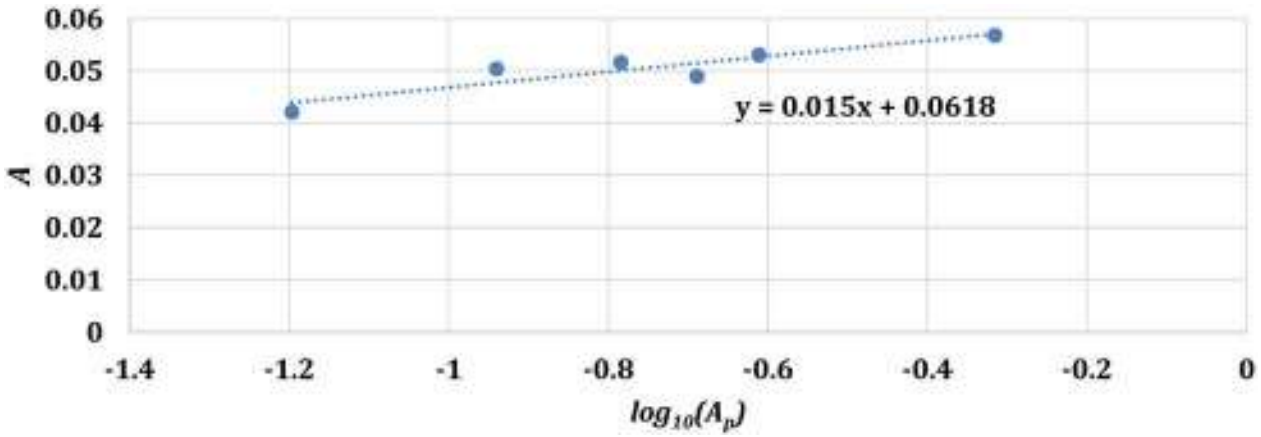

Figure 2—Correlation between parameter A and cross-section area of perforation

Including this effect in the correlation between flow rate and sound pressure level yields:

$$\log(q^3) = A(A_p)L_{SP} + B \tag{3}$$

where

$$A(A_p) = 0.015\log(A_p) + 0.0618 \tag{4}$$

according to trend line from Figure 2. The correlation parameter B does not have an explicit dependence on the perforation diameter as this parameter is recalculated in each time step.

In the system of Equations (2), the parameters $A_1,\ldots,A_n$ are time-dependent variables, because the area of perforation is changing with time. Perforations are growing with different rates of enlargement. Thus, the parameters $A_1,\ldots,A_n$ are dissimilar between clusters as well as between different moments of time. These variations influence the flow and proppant rates of the system, but it demands the computation and update of the perforation diameters on each time step. The model for this diameter recalculation and the enhancement of the previously obtained DAS based interpretation method is developed for DAS interpretation.

Model Development

To correctly predict flow distribution from DAS measurement, we developed a model that estimates perforation diameter change due to erosion as a function of injection volume and the orientation of the perforations.

Proppant Concentration Effect

The rate of proppant passing through a perforation during fracturing affects the rate at which the perforation erodes. The research of Almulhim and others (Almulhim et al., 2020) concluded that the proppant does not effectively turn to the perforations at the heel portion of an interval due to the high inertial effect, and thus the distribution of proppant becomes toe-biased. The mass flow rate of proppant into each perforation cluster is then:

$$\begin{cases} w_{p,1}(t) = c_{p,1}(t) * N_1 q_1(t) \\ \vdots \\ w_{p,n}(t) = c_{p,n}(t) * N_n q_n(t) \end{cases} \tag{5}$$

It is necessary to find the proppant concentration entering each perforation cluster $c_{(p,i)}$ during fracturing treatment to account for the uneven distribution of proppant to each cluster in an interval. CFD simulations were conducted using the ANSYS Fluent software by modeling a proppant and water mixture flow in the 3D pipe (Figure 3) with 15 ft cluster spacing. Each cluster was represented by one perforation with diameters of 0.42 in. One end of the pipe is closed, representing a plug set in the wellbore.

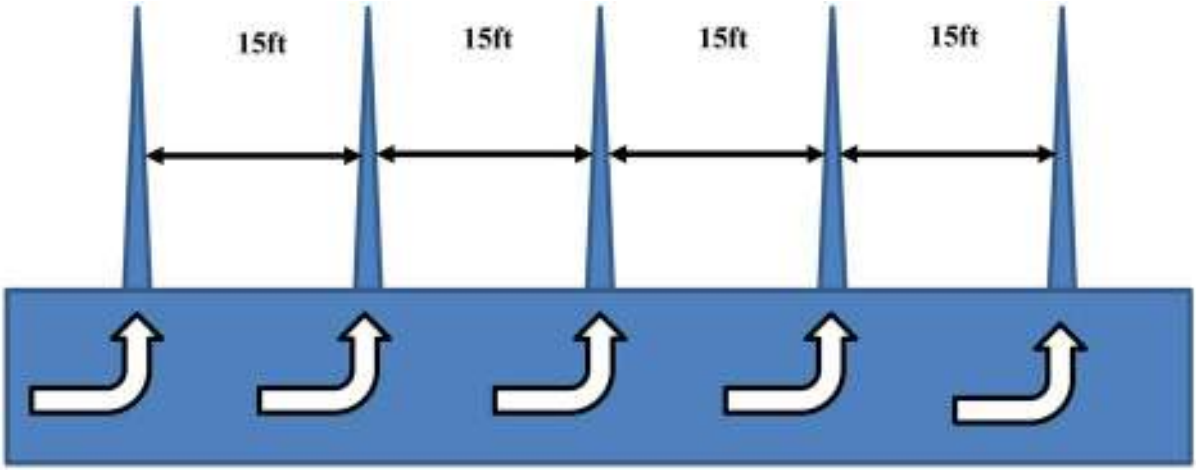

Figure 3—Geometry model for fluid/proppant mixture CFD simulation

The mixture consists of liquid water and proppant in this case. The inlet boundary condition is the fracture fluid flow rate of 90 bpm and the proppant concentration. Different injection proppant concentrations (0.5 lb/gal, 2 lb/gal, 3 lb/gal) were considered in order to estimate the dependency between initial concentration and distribution variations. Based on the application of the described model, the behavior of the mixture flow could be illustrated as an example for cases with 5 clusters per stage and 10 clusters per stage by velocity profiles (Figure 4) along the wellbore. This example is for 2 lb/gal proppant concentration. These profiles show the decreasing inertial effect in the toe direction of the wellbore.

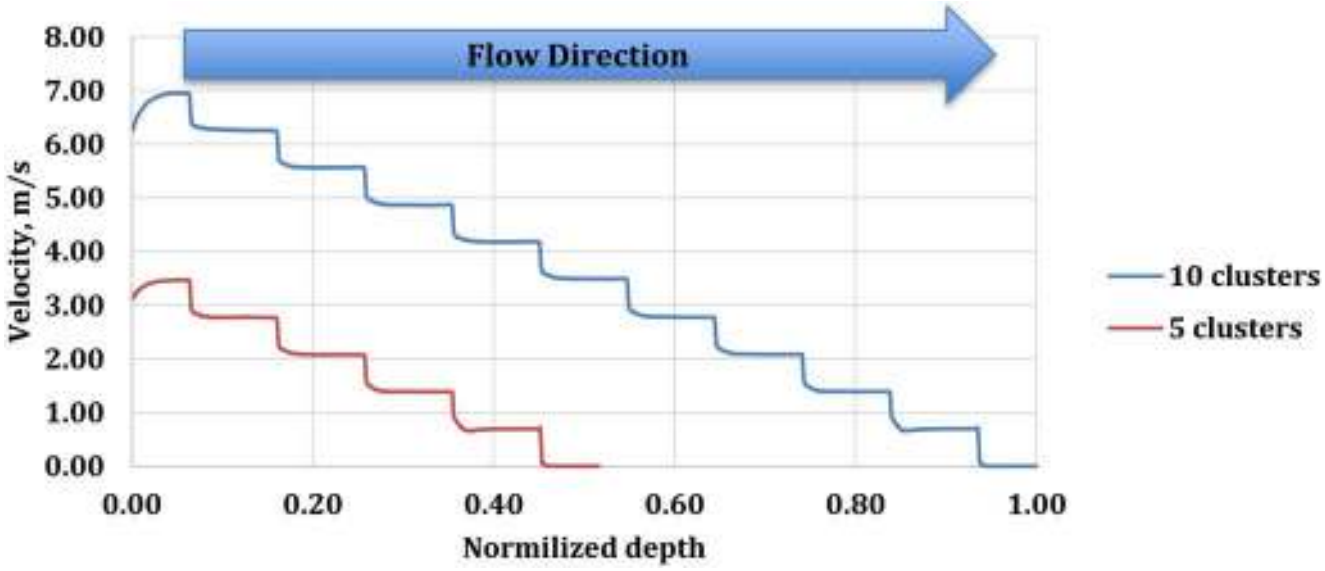

Figure 4—Velocity profiles across the wellbore

The distributions of the normalized mass flow of fluid and proppant for these simulations are visualized as Figure 5 for 5 clusters and Figure 6 for 10 clusters, respectively. Clusters are numbered from toe-side to the heel-side. The fracture fluid distribution is close to uniform, while the proppant distribution is increasing to the toe side of the wellbore. However, for the 10 cluster case, the most toe-ward cluster has less proppant, apparently because of its nearness to the plug.

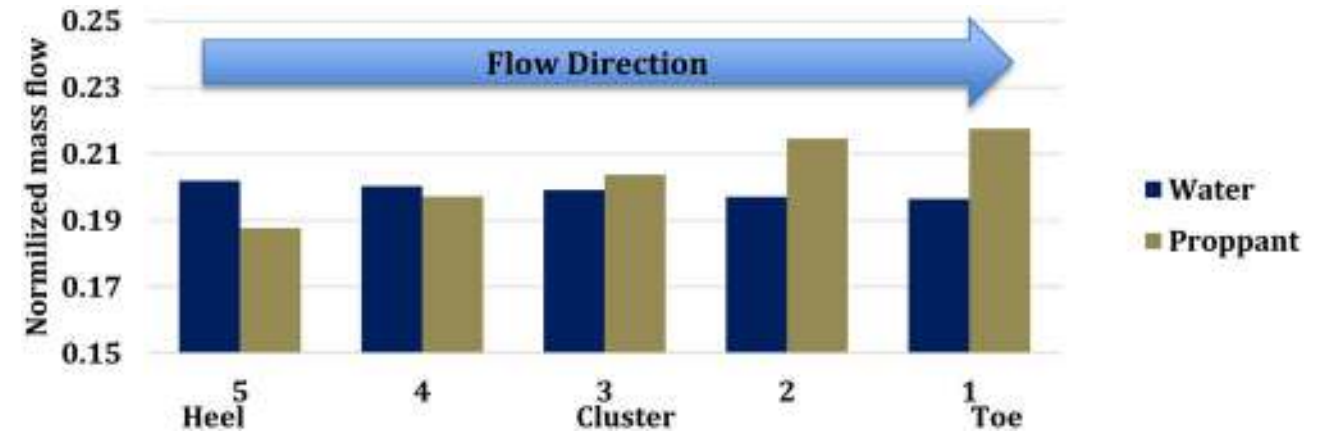

Figure 5—Flow distribution for 5 clusters per stage model

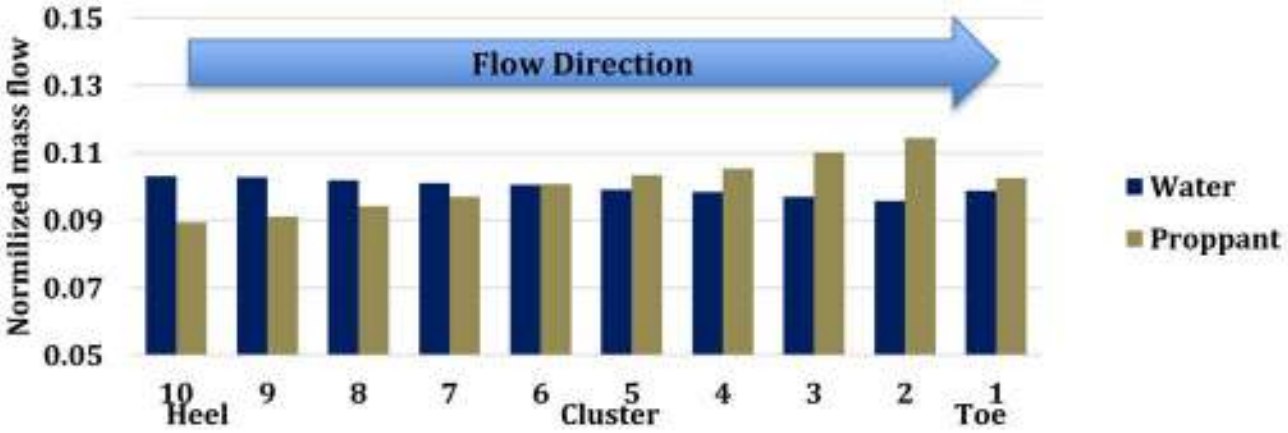

Figure 6—Flow distribution for 10 clusters per stage model

The proppant distribution is not uniform because of the toe-biased proppant concentration. It is illustrated in Figure 7 by average values of concentration for both cases of 5 and 10 clusters. The toe cluster in the 10 clusters case (normalized depth = 1) is eliminated from consideration and assumed equal to the bottomhole value. The modified concentration could be described by the linear function of normalized distance:

$$c_p' = (aL + b) * c_p \tag{6}$$

where c_p' – modified concentration, c_p – injection (bottomhole) concentration, L – normalized distance along the wellbore, a,b – parameters of correlation, depending on the number of clusters:

$$\begin{aligned} a &= 0.039 * n - 0.01 \\ b &= -0.02 * n + 1 \end{aligned} \tag{7}$$

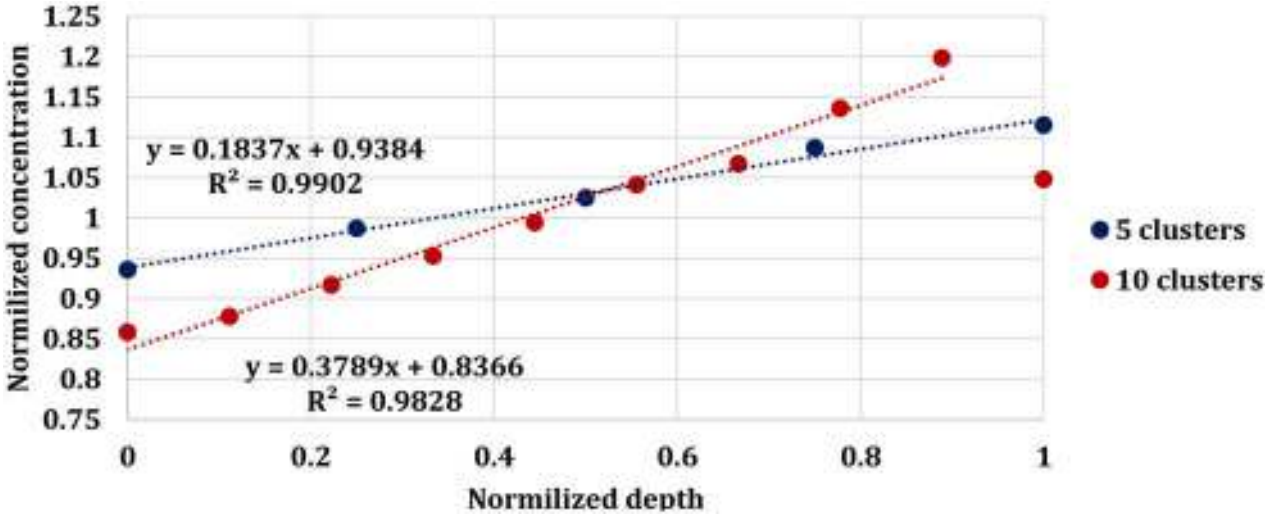

Figure 7—Proppant concentration distribution

In order to improve accuracy of the computation of the existing proppant distribution in the DAS based interpretation method, the obtained correlations are used for the modification of the system of Equations (5):

$$\begin{cases} w_{p,1}(t) = (aL_1 + b) c_p(t) * N_1 q_1(t) \\ \vdots \\ w_{p,n}(t) = (aL_n + b) c_p(t) * N_n q_n(t) \end{cases} \tag{8}$$

These updated proppant mass rates are used in the further calculation of perforation diameters.

Erosion Effect

Diameters of perforations are directly related to the mass of proppant passing through them (Cramer, 1987). In this work, the term hydraulic diameter was used, which is connected with real diameter by the equation:

$$D = \frac{H}{C_d^{0.5}} \tag{9}$$

where D – real perforation diameter, H – hydraulic diameter, C_d – discharge coefficient (parameter responds to the roundness of the hole).

As shown in Figure 8, Cramer (1987) empirically obtained the relationship between the mass of proppant and the hydraulic diameter:

$$\frac{dH}{dt} = \frac{w_p * 0.00418}{1000} \tag{10}$$

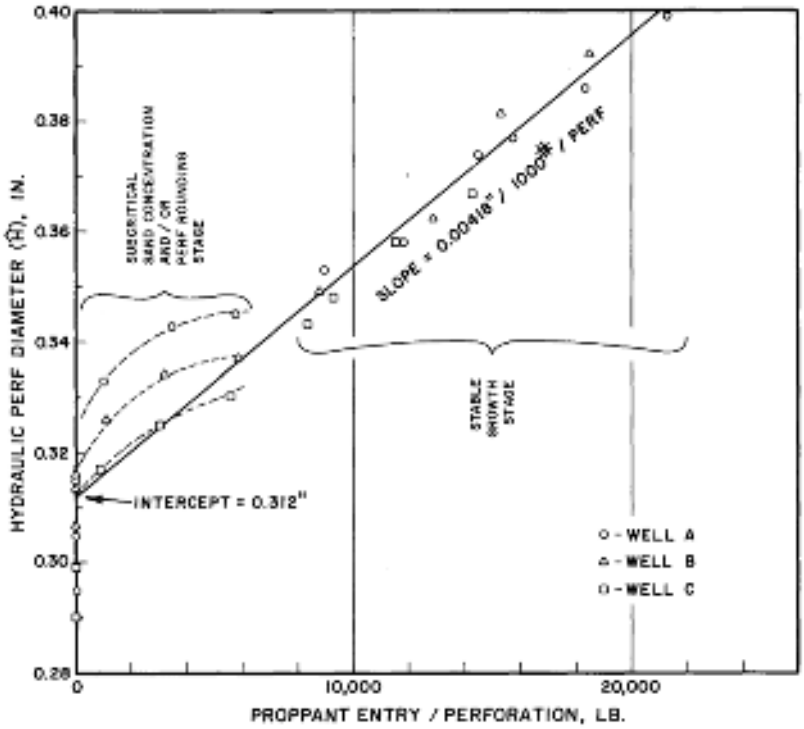

Figure 8—Empirical correlation between proppant flow and hydraulic diameter (Cramer, 1987)

Previous studies of perforation friction and erosion (Cramer et al., 2019, Romero et al., 1995, Willingham et al., 1993) have shown that the discharge coefficient is initially about 0.75, then increase to as high as 0.95 as perforations eroded. Based on these studies, we assume that the relationship between discharge coefficient and mass of proppant is:

$$C_d = \begin{cases} 3.5 * 10^{-4} * \frac{W_{cum}}{N} + 0.75, \text{if } W_{cum} < 600lb \\ 0.95, \text{if } W_{cum} \geq 600lb \end{cases} \tag{11}$$

This research proposes a modification of the relationship between the hydraulic diameter and proppant rate with the effect of the velocity of flow:

$$H(t + \Delta t) = H(t) + \alpha \left(\frac{w_p(t)}{1000 * N} v(t) \right)^{\beta} \Delta t \tag{12}$$

where t – time, v – velocity, α and β – parameters of correlation.

The actual diameter is:

$$D(t+\Delta t) = D(t) + \frac{\alpha\left(\frac{w_p(t)}{1000^* N} v(t)\right)^{\beta} \Delta t}{\left(C_d(t)\right)^{0.5}} \tag{13}$$

Perforation Orientation Effect

Another factor that influences the diameter growth is perforation orientation, which is the angle φ between perforation direction and the vertical axis with φ = 0 at the top of the casing, as shown in Figure 9.

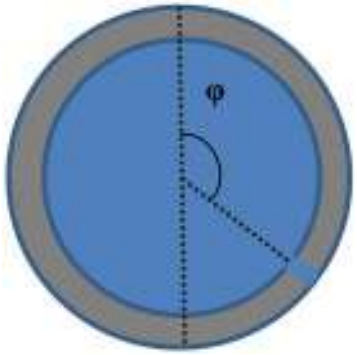

Figure 9—Perforation orientation

Based on the results of empirical research (Roberts et al., 2020), perforations with angle φ equal to 180° (at the bottom of the casing) have the most significant erosion rate, which is decreasing with deviation from this angle in both directions of rotation. This conclusion is illustrated in Figure 10.

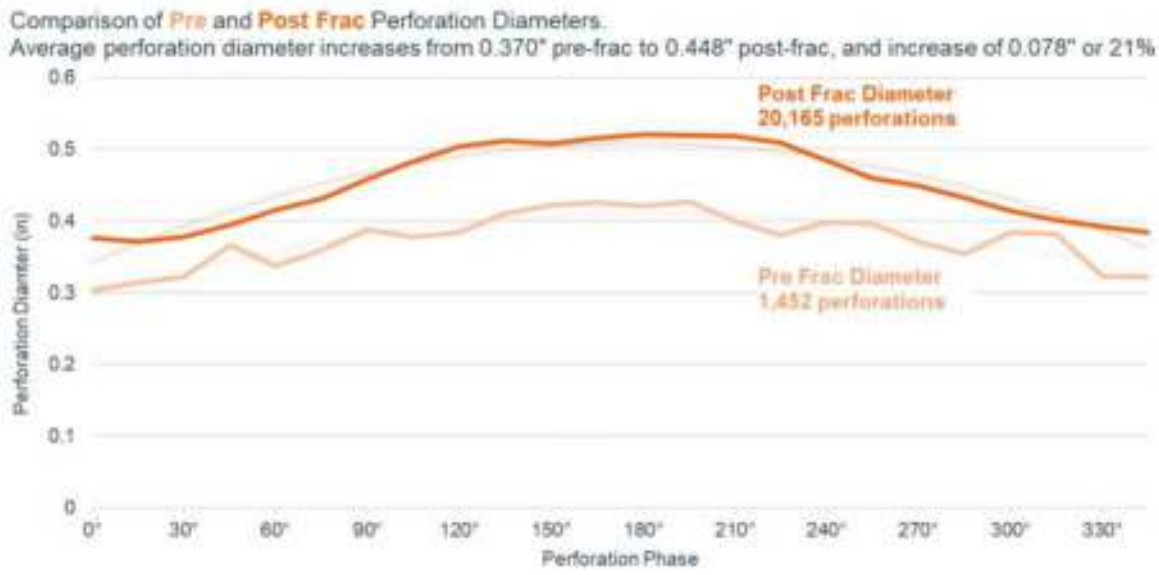

Figure 10—Pre-frac and post-frac perforation diameter as a function of perforation orientation (Roberts et al., 2020)

In order to implement the results of this observation, an additional correction function γ is developed and applied to the equation of diameter (Equation (13) by multiplication of numerator by this correction function:

$$\gamma = \begin{cases} 8\left(\dfrac{e^{-\frac{(\varphi-180)^2}{2*15^2}}}{(\varphi+68)(428-\varphi)t_{inj}}\right)^{0.1}, |\varphi-180| < 20 \\ 1, |\varphi-180| \geq 20 \end{cases} \quad (14)$$

where t_{inj} – time of proppant injection during the stage of consideration. This function contains a component proportional to the normal distribution due to the curvature in Figure 10. Another component is based on the rate of the diameter growth depending on the perforation angle based on the results from Figure 10. This correction function is shown in Figure 11.

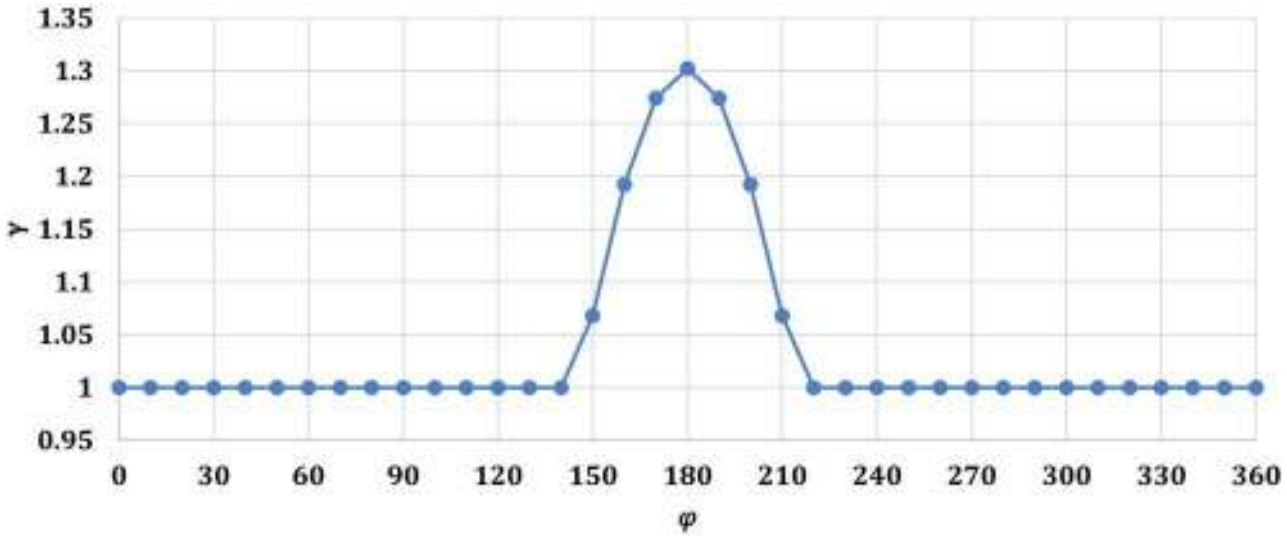

Figure 11—Correction factor based on perforation orientation

The final modified diameter after the consideration of concentration, erosion, and orientation effects is formulated as

$$D'(t+\Delta t) = D'(t) + \frac{\alpha\gamma\left(\frac{w_p(t)}{1000*N}v(t)\right)^{\beta}\Delta t}{C_d^{0.5}} \quad (15)$$

The overall DAS interpretation method is detailed in the flowchart shown in Figure 12. The model demands input information, which includes initial perforation's diameters $D_{i\,(t_0)}$, perforation orientations φ_i, total number of perforations N_{tot} and their clusters distribution, time of proppant injection t_{inj}, and total mass of proppant injected during the stage W_{tot}. The proppant concentrations for each cluster are calculated by Equation (6). Based on the diameters of perforations the area of perforations is recalculated at each time step and used in order to find parameters of correlation A_i in Equation (4). Using these parameters, the flow rates are calculated according to the system of Equations (2). The resulting flow rates are used in the calculation of proppant mass rates by the system of Equations (8) and velocities of fluid passing through perforations. The updated diameter after the time step is recalculated by Equation (15) using parameters α and β along with correction factor γ. The updated perforation diameters are used for the flow rate and proppant rate calculations in the next time step.

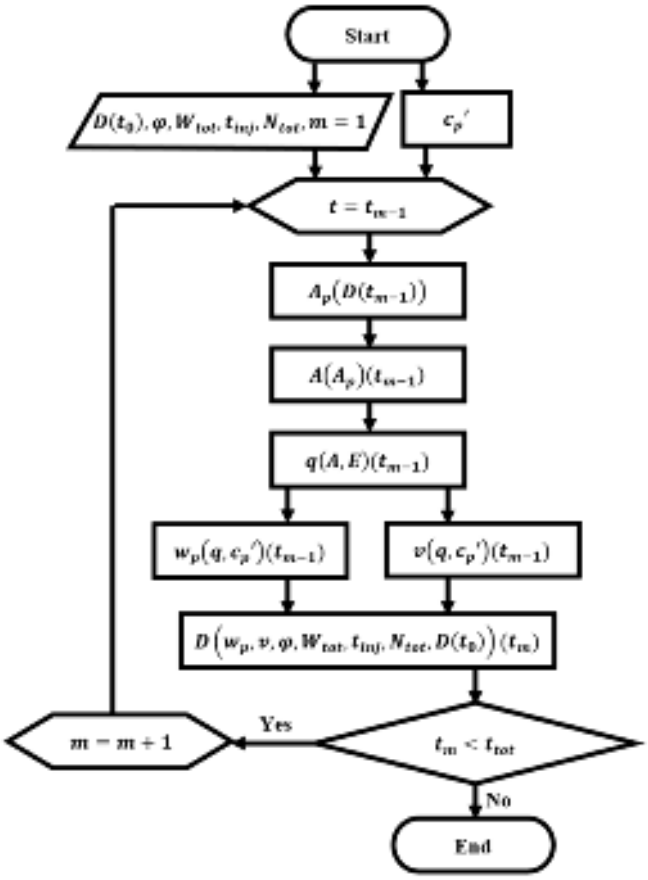

Figure 12—Flowchart of the modified DAS based interpretation method

Validation of modified DAS based interpretation method

To apply the interpretation method, we must estimate the parameters α and β in Equation (14). Estimation of these parameters is based on the case presented by Cramer et al. (2019). This example is used as it has information about perforation sizes before and after fracturing, along with the DAS signal (Figure 13). This example is for a stage of fracturing with 5 perforation clusters in a horizontal wellbore with a pumping schedule provided by Figure 14. Perforation clusters locations are denoted by green triangles along the depth axis. The red square responds to the plug set position. The clusters of this example have the configuration described in Table 2. It is assumed that shot orientation angle equal to 335° as it is described in Cramer's paper: "all perforations in Frac Stage 21 were located within a 10° phasing range (i.e., 20° to 30° from the wellbore high point)". The assumed position of the perforations is shown in Figure 15.

Table 2—Stage parameters

Stage	Cluster count	Cluster depth	Shot count	Shot orientation
21	5	8290	4	335
		8325	4	335
		8361	6	335
		8401	6	335
		8432	8	335

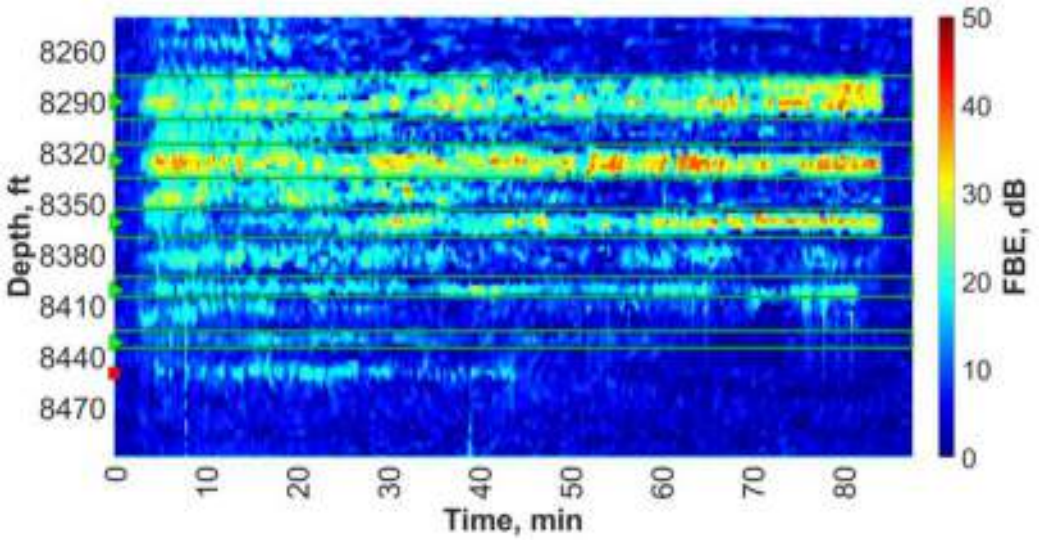

Figure 13—DAS waterfall plot

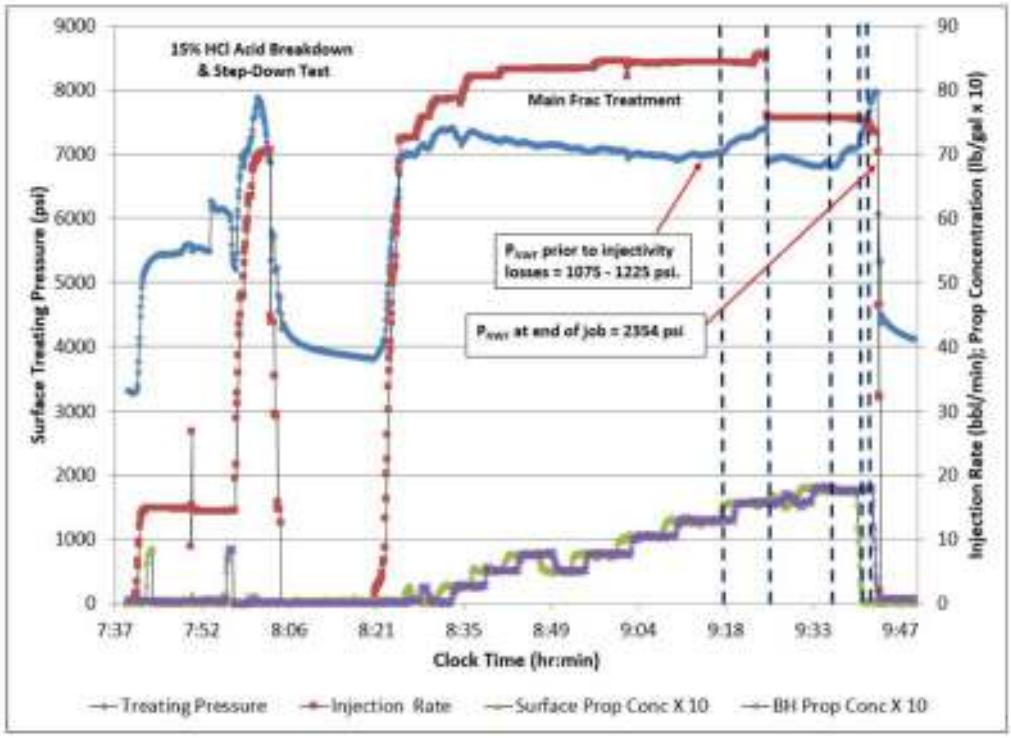

Figure 14—Pumping schedule (Cramer et al., 2019)

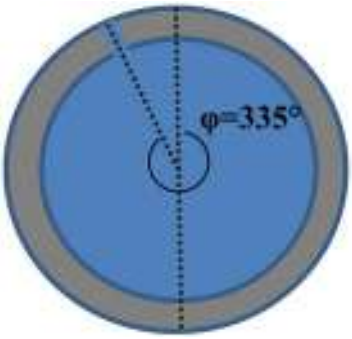

Figure 15—Perforation orientation in the example from Cramer's paper

Initially, the correction parameter γ is not used in the validation procedure. Knowing the resulting diameters from visual observation, it is necessary to specify such parameters α and β, that deliver the minimum for the minimization function, F_{min}:

$$F_{\min} = \left(D_1 - D_1^*\right)^2 + \cdots + \left(D_n - D_n^*\right)^2 \tag{16}$$

where $D_1,\ldots,D_n$ – diameters calculated by the interpretation method, $D_1^*,\ldots,D_n^*$ – diameters from the video-based observations of real perforations. With a variation of parameter α in the range from 1e-6 to 1e-4, it is possible to find the minimization function value for different β in the Equation (15), as shown in Figure 16.

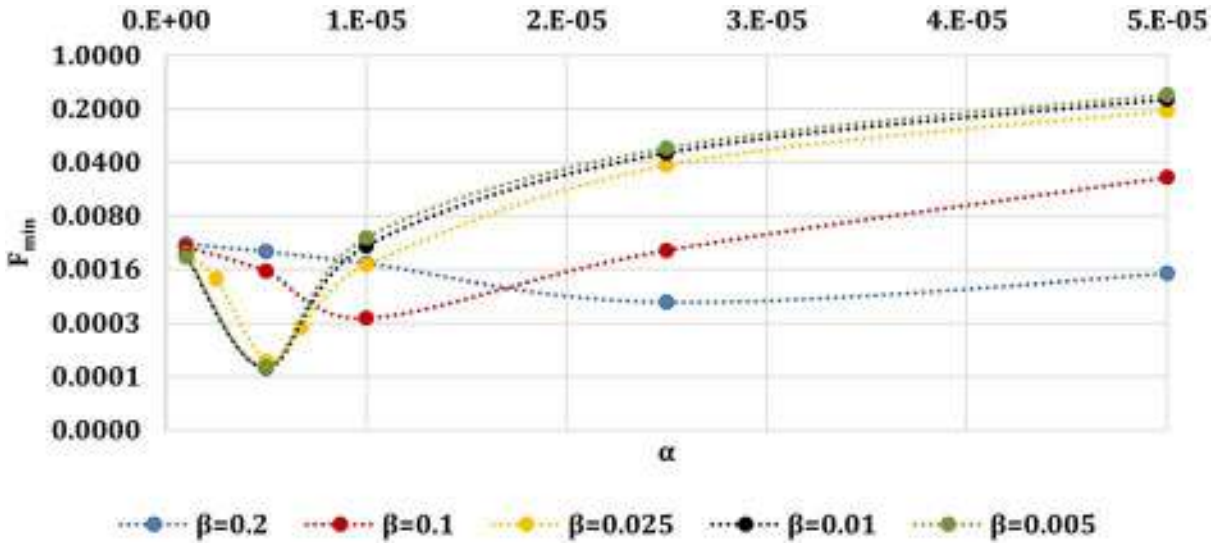

Figure 16—Estimation of the parameter # from Cramer's paper

By comparison of the response curves with different values of β, it is concluded that the minimum value of F_{min} is attained with enough accuracy level at β =0.025. Further reduction of β does not provide significant improvement of the minimization function. Therefore, the correlation of diameter takes the form:

$$D(t+\Delta t) = D(t) + \frac{\alpha\gamma\left(\frac{w_P(t)}{1000*N}v(t)\right)^{0.025}\Delta t}{C_d^{0.5}} \tag{17}$$

Based on the empirical observations of a variety of DAS examples, it is concluded that coefficient α could depend on many parameters. These parameters include the total number of perforations per stage N_{tot}, the total mass of pumped proppant W_{tot}, and the time of injection t_{inj}. The dependency could be represented as the power function shown in Figure 17 and described by the equation:

$$\alpha = 4.3*10^{-15}*\left(\frac{W_{tot}}{N_{tot}t_{inj}}\right)^{4.32} \tag{18}$$

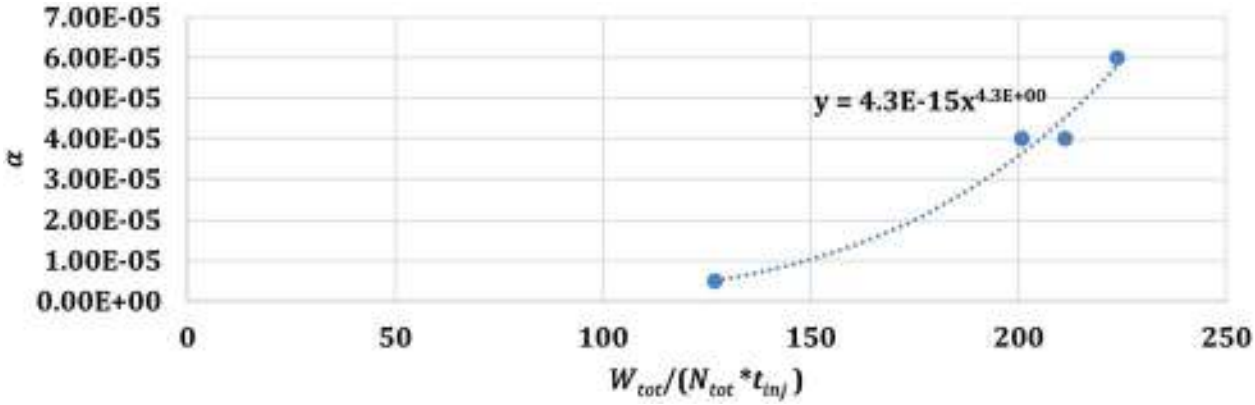

Figure 17—Estimation of the parameter #

Implementation of Equation (18) to Equation (17) with the usage of correction factor γ provides the final **Equation ()**, which allows a better estimation of the eroded diameter of perforations.

$$D(t+\Delta t) = D(t) + \frac{4.3*10^{-15}*\left(\frac{W_{tot}}{N_{tot}t_{inj}}\right)^{4.32}\gamma\left(\frac{w_p(t)}{1000*N}v(t)\right)^{0.025}\Delta t}{C_d^{0.5}} \tag{19}$$

The application of **Equation ()** to the example from Cramer's paper is shown in Figure 18. Figure 18 shows that the effect of perforation orientation is insignificant. In case the information is not available, the correlation presented in the paper can still be used to estimate perforation diameter with erosion effect.

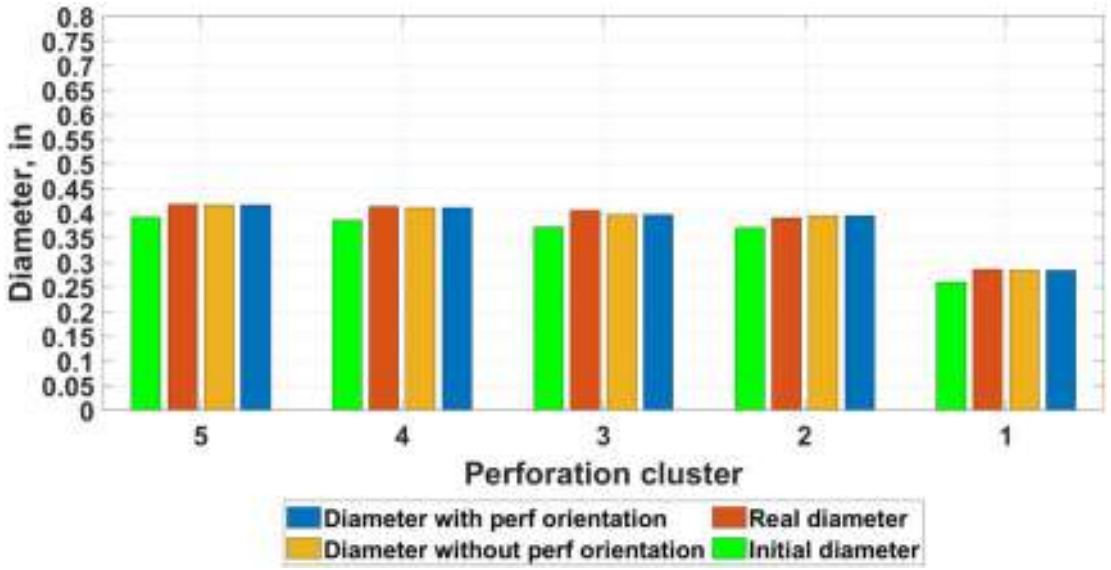

Figure 18—Perforation sizes generated by the correlations

In order to analyze how erosion affects the fluid and proppant distributions, the full interpretation procedure was applied, and the distributions were computed, as shown in Figure 19 for fluid flow and Figure 20 for proppant, respectively. For this case, it appears that the small growth in perforation diameters that occurred had a negligible effect on either the fluid or the proppant distributions. This is consistent with the modeling predictions of Long and Xu (2017).

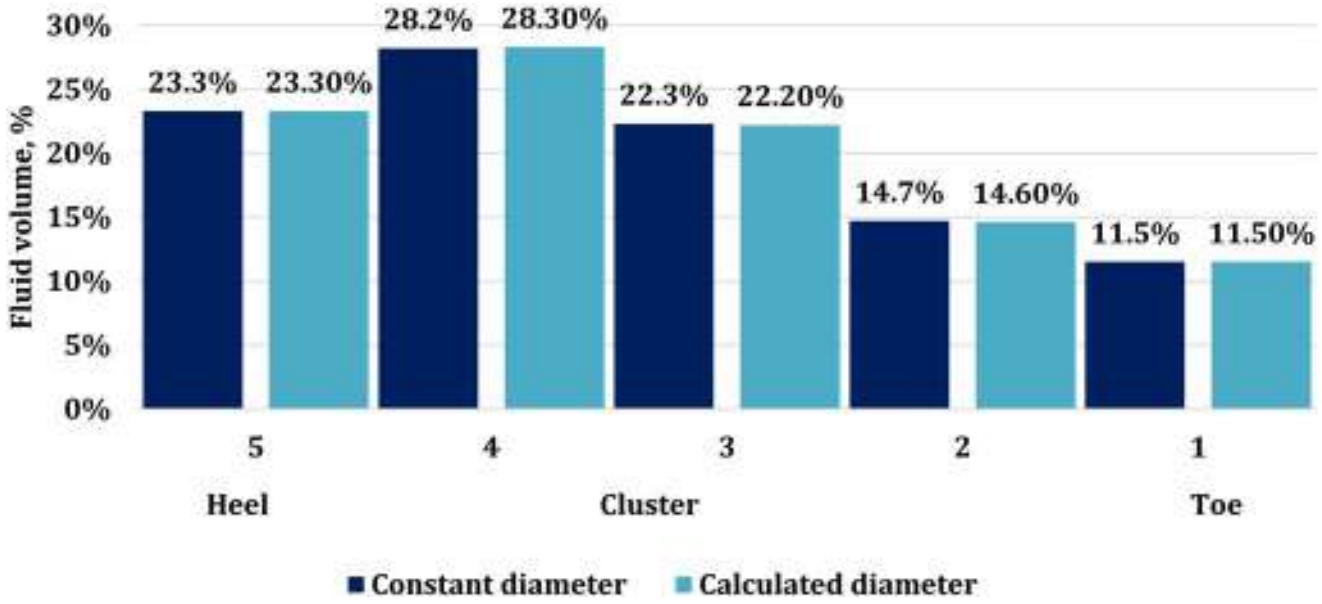

Figure 19—Erosion effect on the fluid distribution

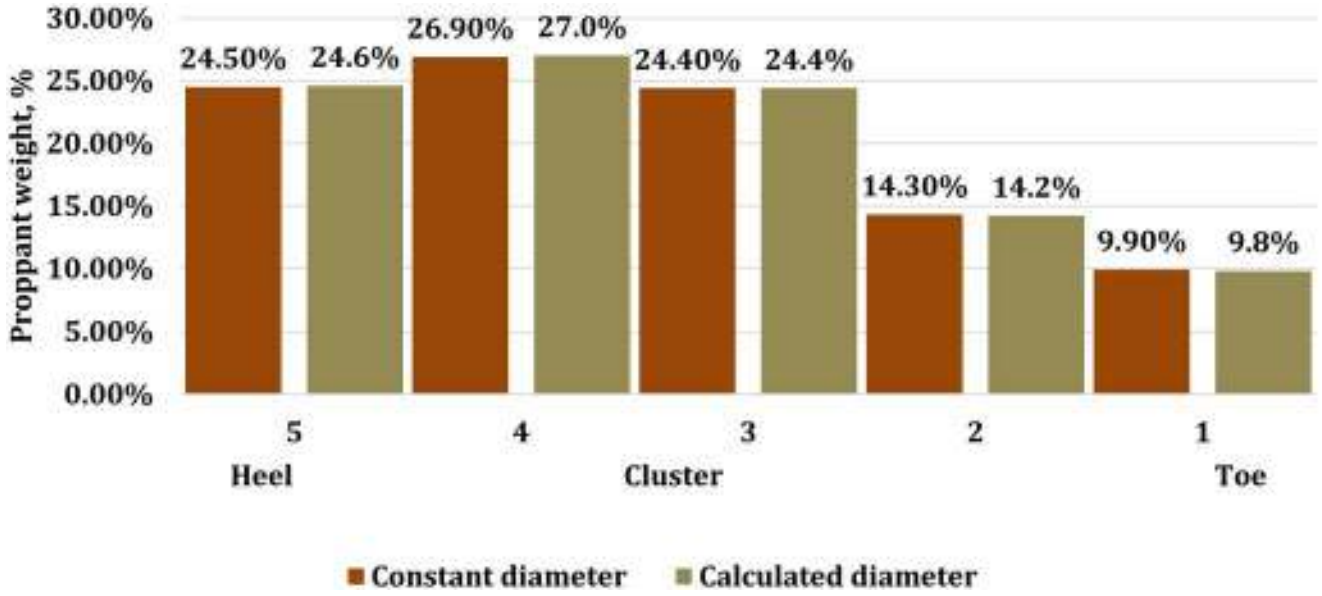

Figure 20—Erosion effect on the proppant distribution

Application of DAS interpretation method to the MSEEL data

The DAS interpretation method was applied to the Marcellus Shale Energy and Environment Laboratory (MSEEL) data. This field site is located in West Virginia near Morgantown across the Monongahela River. The geographical location of MIP-3H wellbore is shown on the map (Figure 21).

Figure 21—Marcellus Shale Energy and Environment Laboratory (Amini et al. 2017)

All the stages of the MIP-3H well, which have reasonably high-quality DAS data and pumping schedules, were interpreted in this work. The configuration of clusters, including the number of shots per cluster and perforation orientation, are provided in Table 3.

Table 3—Stages parameters for MIP-3H wellbore

Stage	Cluster depth	Shot count	Shot orientation
28	7,753	8	297
	7,803	8	259
	7,852	8	300
	7,901	8	318
27	7,944	8	294
	7,993	8	305
	8,042	8	317
	8,085	8	308
26	8,128	8	318
	8,175	8	293
	8,220	8	302
	8,264	8	291
	8,310	8	297
25	8,356	8	293
	8,400	8	309
	8,448	8	301
	8,495	8	264
	8,541	8	265
24	8,587	8	293
	8,634	8	292
	8,678	8	302
	8,724	8	297
	8,763	8	307
23	8,814	10	288
	8,863	10	295
	8,910	10	285
	8,959	10	284
	9,005	10	310
22	9,051	10	310
	9,087	10	304
	9,136	10	308
	9,183	10	294
	9,227	10	290
21	9,271	8	302
	9,318	8	302
	9,365	8	319
	9,410	8	298
	9,445	8	278
20	9,504	8	286
	9,552	8	300
	9,594	8	303
	9,639	8	280
	9,685	8	309
19	9,732	6	296
	9,779	6	320
	9,823	6	306
	9,869	6	303
18	9,912	8	297
	9,959	8	303
	10,002	8	301
	10,048	8	325
16	10,278	6	302
	10,316	8	290
	10,365	6	303
	10,408	6	306
15	10,456	6	305
	10,503	6	308
	10,547	8	308
	10,594	6	304
13	10,863	6	307
	10,909	6	310
	10,955	6	309
	11,000	6	302
	11,046	6	308
10	11,557	10	303
	11,601	10	299
	11,649	10	311
	11,695	10	299
	11,735	10	302
8	12,015	10	293
	12,058	10	283
	12,098	10	327
	12,143	10	308
	12,194	10	308
7	12,239	10	309
	12,285	10	303
	12,325	10	308
	12,367	10	308
	12,418	10	296
2	13,398	10	305
	13,443	10	291
	13,490	10	295
	13,532	10	272
	13,576	10	257

The final eroded diameters are calculated and vary from stage to stage, as shown in Figure 22. The initial diameter is assumed to be the designed specification of 0.42 in, marked by the red dashed horizontal line. In most of the stages, the diameter growth is less than 0.1in.

More significant growth of stage 19 diameter sizes was caused by the stage design, which has only 4 clusters with a reduced number of perforations per cluster (6 shot/cluster) in comparison with other stages. It induces more massive proppant movement and increased erosion. In stage 27, the total mass of the injected proppant was higher than any of other stages, explaining the high diameter growth in this stage interval.

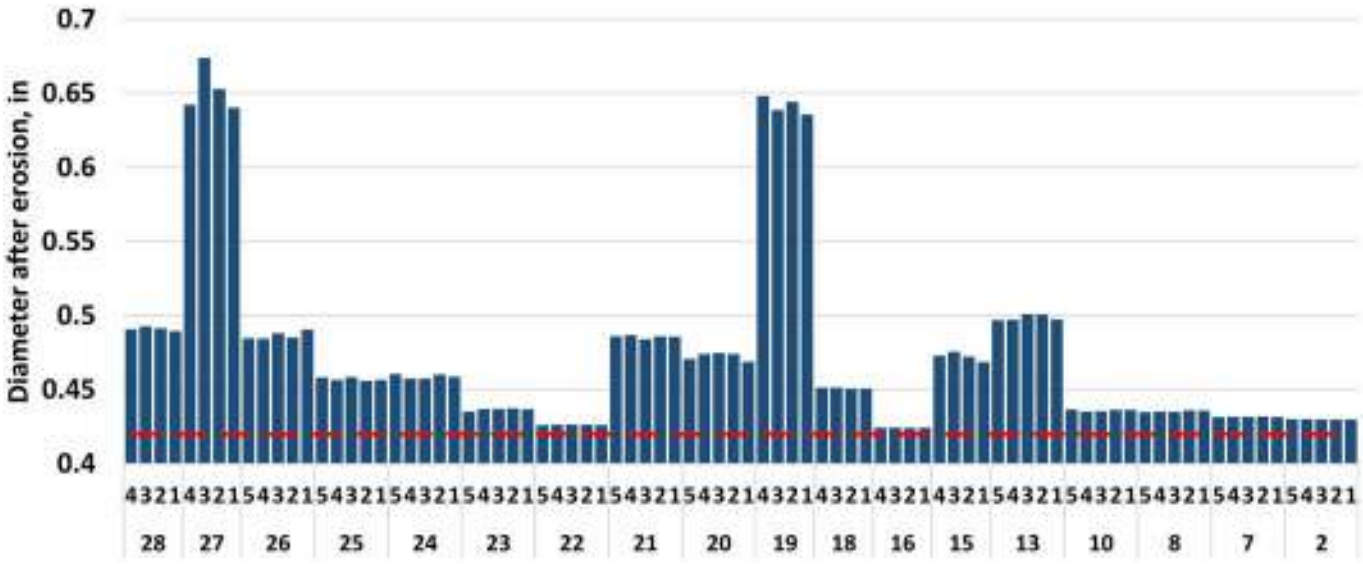

Figure 22—Eroded diameters for MSEEL data

The DAS data also allows the calculation fluid and proppant profiles after the hydraulic fracturing treatment by calculation of the cumulative volume of fluid and cumulative mass of proppant, which gives an estimation of fracturing effectiveness. During this procedure, the new fluid and proppant distributions are calculated and demonstrated in Figure 23 and Figure 24 as a comparison between the non-eroded case and modified model with erosion effect. From the observation of Figure 23 and Figure 24, it is noticed that the variation of fluid and proppant distribution is only observable in stages 19 and 27 and the difference caused by erosion is only 1-2%. All other stages show very similar fluid and proppant distribution with or without erosion effect. Somewhat surprisingly, erosion does not appear to have a significant effect on fluid and proppant distribution for the case studied. For this example, we assumed the same initial perforation hole size (the gun size) for all perforation holes. In reality, initial perforation hole size is likely varying even if all perforating charges are identical. A variation in initial perforation hole sizes might change these conclusions about the effects of erosion. If that is not the case, it appears that other factors, such as near well tortuosity, may have more effect on the DAS response than the perforation hole size, as suggested by Ugueto et al. (2019).

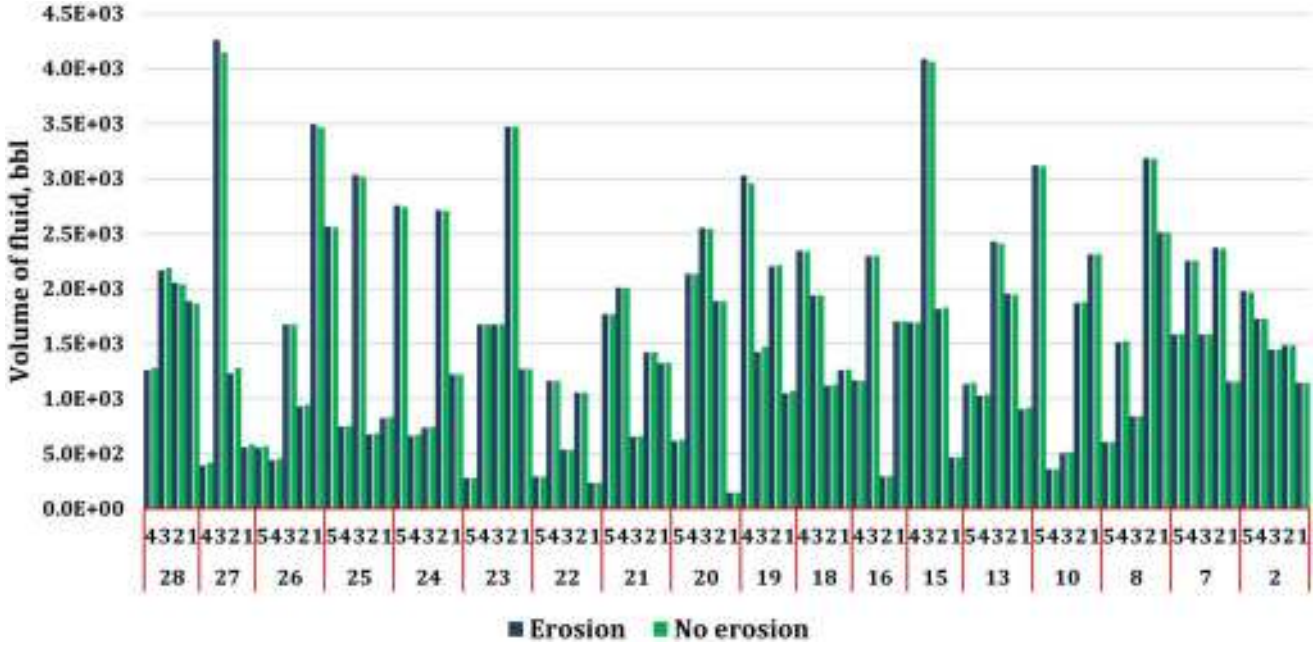

Figure 23—Fluid volume distribution (modified interpretation method)

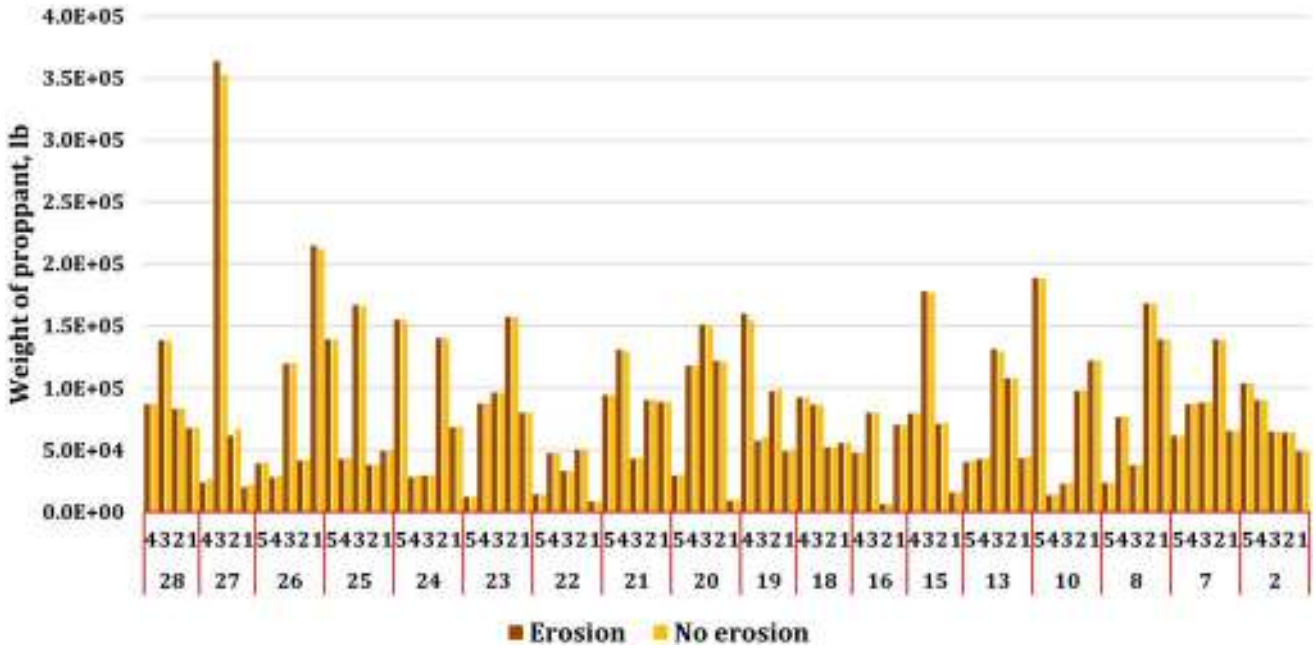

Figure 24—Proppant mass distribution (modified interpretation method)

Conclusions

The modified DAS-based interpretation method allows calculating fluid and proppant distribution along with estimations of the diameters of eroded perforations during a hydraulic fracturing treatment. Completion design characteristics, such as the number of perforations per clusters, number of clusters, perforation orientation, initial perforation size as well as proppant concentration, time of proppant pumping influence the erosion effect and subsequent diameter of eroded perforations. All of these parameters are incorporated into the developed interpretation method. Parameters in our model of perforation erosion were tuned using Cramer's data that included before and after fracturing perforation diameters and DAS data.

We used our model to interpret the DAS data measured during fracturing of the MSEEL MIP-3H well. Our model of perforation erosion in this well showed that perforations were significantly eroded in only two stage intervals in this well. Significantly more proppant per perforation was pumped in these 2 stages than was placed in the other stages, causing the greater amount of erosion.

The calculated distribution of both fracture fluid and proppant was extracted from the DAS response, including the effect of perforation erosion. Comparing the fluid and proppant distributions obtained including changing perforation diameters with the distributions calculated assuming constant perforation diameters throughout fracturing showed that perforation erosion had a slight effect of fluid and proppant distribution.

Nomenclature

A,B parameters of correlation between DAS signal and flow rate;
A_p area of perforation cross-section;
α,β parameters of correlation for hydraulic diameter;
γ perforation orientation correction factor;
C_d discharge coefficient;
c_p bottomhole proppant concentration (PPA);
c'_p modified proppant concentration (PPA);
$c_{(p,i)}$ proppant concentration in cluster i (PPA);
D equivalent perforation diameter, (in);
D_i equivalent perforation diameter in cluster *i*, (in);
D_i* equivalent perforation diameter in cluster i from video-based perforation imaging, (in);
E frequency band energy (Db);
E_i FBE in cluster i (Db);
F_{min} minimization function for perforation diameter;
H hydraulic perforation diameter (in);
L_i normalized distance to the position of cluster i;
L_{SP} sound pressure level (Db);
N number of perforations per cluster;
N_i number of perforations per cluster i;
N_{tot} total number of perforations per stage;
n total number of perforated clusters in one stage;
q flow rate (bbl/min);
q_i flow rate in one perforation in cluster i (bbl/min);
q_T total flow rate of fluid injected for fracturing treatment (bbl/min);
t time (min);
t_{inj} time of proppant pumping (min);
v velocity (m/s);
w_p mass of proppant (lb);
$w_{(p,i)}$ mass of proppant injected in cluster i (lb);
W_{cum} the cumulative mass of proppant pumped in cluster, (lb);
W_{tot} the total mass of proppant pumped in stage, (lb);
φ perforation orientation

References

Almulhim, A., Kebert, B., Miskimins, J., Hunter, W., & Soehner, G. (2020, January 28). Field-Scale Computational Fluid Dynamics CFD Modeling of Proppant Transport and Distribution Within a Horizontal Hydraulic Fracturing Stage. *Society of Petroleum Engineers*.10.2118/199727-MS

Amini, S., Kavousi, P., & Can, T. R. (2017, July 24). Application of Fiber-optic Temperature Data Analysis in Hydraulic Fracturing Evaluation: A Case Study in Marcellus Shale. Unconventional Resources Technology Conference. 10.15530/URTEC-2017-2686732

Chen, K., Zhu, D., & Hill, A. D. (2015, September 28). Acoustic Signature of Flow From a Fractured Wellbore. *Society of Petroleum Engineers*.10.2118/174877-MS

Cramer, D. D. (1987, January 1). The Application of Limited-Entry Techniques in Massive Hydraulic Fracturing Treatments. *Society of Petroleum Engineers*. 10.2118/16189-MS

Cramer, D., Friehauf, K., Roberts, G., & Whittaker, J. (2019, January 29). Integrating DAS, Treatment Pressure Analysis and Video-Based Perforation Imaging to Evaluate Limited Entry Treatment Effectiveness. *Society of Petroleum Engineers*.10.2118/194334-MS

Long, G., & Xu, G. (2017, April 1). The Effects of Perforation Erosion on Practical Hydraulic-Fracturing Applications. *Society of Petroleum Engineers*. 10.2118/185173-PA

Pakhotina, I., Sakaida, S., Zhu, D., & Hill, A. D. (2020, January 28). Diagnosing Multistage Fracture Treatments with Distributed Fiber-Optic Sensors. *Society of Petroleum Engineers*. 10.2118/199723-MS

Pakhotina, J., Zhu, D., Hill, A. D., & Santos, R. (2017, October 9). Characterization of Production through a Fracture Cell Using Acoustic Data. *Society of Petroleum Engineers*. 10.2118/187357-MS

Roberts, G., Whittaker, J., McDonald, J., & Paxson, T. (2020, January 28). Proppant Distribution Observations from 20,000+ Perforation Erosion Measurements. *Society of Petroleum Engineers*.10.2118/199693-MS

Romero, J., Mack, M. G., & Elbel, J. L. (1995, January 1). Theoretical Model and Numerical Investigation of Near-Wellbore Effects in Hydraulic Fracturing. *Society of Petroleum Engineers*. doi:10.2118/30506-MS

Ugueto, G., Huckabee, P., Wojtaszek, M., Daredia, T., & Reynolds, A. (2019, January 29). New Near-Wellbore Insights from Fiber Optics and Downhole Pressure Gauge Data. *Society of Petroleum Engineers*. 10.2118/194371-MS

Willingham, J. D., Tan, H. C., & Norman, L. R. (1993, January 1). Perforation Friction Pressure of Fracturing Fluid Slurries. *Society of Petroleum Engineers*. doi:10.2118/25891-MS